RESEARCH ARTICLE

WILEY

Tanshinone IIA combined with cisplatin synergistically inhibits non-small-cell lung cancer in vitro and in vivo via down-regulating the phosphatidylinositol 3-kinase/Akt signalling pathway

Xiao-Zhong Liao[1,2] | Ying Gao[2] | Sheng Huang[3] | Zhuang-Zhong Chen[1] | Ling-Ling Sun[1] | Jia-Hui Liu[2] | Han-Rui Chen[1] | Ling Yu[1] | Jia-Xing Zhang[2] | Li-Zhu Lin[1] (iD)

[1] Department of Oncology, The First Affiliated Hospital of Guangzhou University of Chinese Medicine, Guangzhou, China

[2] Department of Oncology, The First Affiliated Hospital, Sun Yat-sen University, Guangzhou, China

[3] Department of Orthopaedic Surgery, The First Affiliated Hospital of Nanchang University, Nanchang, China

Correspondence
Li-Zhu Lin, Department of Oncology, The First Affiliated Hospital of Guangzhou University of Chinese Medicine, Yard 16, Airport Road, Guangzhou 510405, China.
Email: lizhulin26@yahoo.com Jia-Xing Zhang, Department of Oncology, The First Affiliated Hospital, Sun Yat-sen University, Guangzhou 510080, China.
Email: zjxlundy@hotmail.com

Funding information
Natural Science Foundation of Guangdong Province, Grant/Award Number: 2018B030311023; National Natural Science Foundation of China, Grant/Award Numbers: 81573780 and 81702671; Natural Science Foundation of Guangdong, Grant/Award Number: 2018B030311023; Sun Yat-sen University Cancer Center

Cisplatin represents one of the first-line drugs used for non-small-cell lung cancer treatment. However, considerable side effects and the emergence of drug resistance are becoming critical limitations to its application. Combinatorial strategies may be able to extend the use of cisplatin. Both Tanshinone IIA and cisplatin inhibit non-small-cell lung cancer cell growth in a time- and dose-dependent manner. When Tanshinone IIA was combined with cisplatin at a ratio of 20:1, they were observed to exert a synergistic inhibitory effect on non-small-cell lung cancer cells. The combination treatment was shown to impair cell migration and invasion, arrest the cell cycle in the S phases, and induce apoptosis in A549 and PC9 cells in a synergistic manner. KEGG pathway analysis and molecular docking indicated that Tanshinone IIA might mainly influence the phosphatidylinositol 3-kinase-Akt signalling pathway. In all treated groups, the expression levels of Bax and cleaved Caspase-3 were up-regulated, whereas the expression levels of Bcl-2, Caspase-3, p-Akt, and p-PI3K proteins were down-regulated. Among these, the combination of Tan IIA and cisplatin exhibited the most significant difference. Tanshinone IIA may function as a novel option for combination therapy for non-small-cell lung cancer treatment.

KEYWORDS

A549, cisplatin, combination, PC9, PI3K/Akt pathway, synergistic effect, Tanshinone IIA

1 | INTRODUCTION

The incidence and mortality rate of lung cancer are among the highest for all tumours worldwide (Siegel, Miller, & Jemal, 2017). Non-small-cell lung cancer (NSCLC) accounts for 85% of all lung cancer cases and can be classified into three subtypes: squamous cell carcinoma, large cell carcinoma, and adenocarcinoma (Webb & Simon, 2010). Platinum-based chemotherapy is an important adjuvant therapeutic strategy for NSCLC patients (Jin et al., 2016). As the most widely used platinum compound, cisplatin (DDP; Figure 1a) is the first-line chemotherapeutic agent for the treatment of NSCLC and can induce cancer cell cycle arrest and apoptotic cell death (Galluzzi et al., 2014). However, the tremendous side effects caused by chemotherapy and the development of chemoresistance severely impact the efficacy of treatments as well as quality of life, which accounts for the major chemotherapy failure in both resectable and advanced NSCLC (Wohlkoenig et al., 2011), indicating that there is room for improvement in treatment methods. Thus, increasing attention has been focused on traditional Chinese medicine (TCM) to explore new cancer approaches that are promising and effective for patients with NSCLC.

TCM, comprises mainly natural products, has recently attracted increasing public attention, and many researchers have explored novel therapeutic targets against NSCLC. Tanshione IIA (Tan IIA; Figure 1b) represents one of the primary fat-soluble compositions that was isolated from *Salvia miltiorrhiza*, and it is referred to as "Dan-Shen" in TCM. The compound ID of Tan IIA in PubChem compound is 164676.

Tan IIA is prescribed for the treatment of cardiovascular disease in the pharmacopoeia of the People's Republic of China as the TCM "Danshen." Tan IIA has been shown to exhibit antiangiogenic (Tsai, Yang, Wu, Pang, & Huang, 2011), antioxidant (Guo et al., 2018), anti-inflammatory, immunomodulatory (Chen & Xu, 2014), and antitumor activities. A number of studies have shown that Tan IIA antagonizes the proliferation of multiple human cancer cell lines, such as human colorectal cancer (He & Gu, 2018; Sui et al., 2017), human gastric carcinoma (Su, 2018; Zhang et al., 2018), human pancreatic cancer (Chiu & Su, 2017), human breast cancer and (Li & Lai, 2017; Lv et al., 2018), and human osteosarcoma cells (Huang et al., 2017). However, the specific mechanisms of action underlying the anticancer effects of Tan IIA in NSCLC cells remain elusive.

In the present study, the cytotoxic effects of Tan IIA and DDP on NSCLC cells were examined using the Cell Counting Kit-8 assay. The wound healing assay, transwell assay, cell cycle analysis, apoptosis assay, mouse xenograft model, bioinformatics analysis, and western

blotting were carried out to investigate and confirm the mechanism of action in A549 and PC9 cells following Tan IIA, DDP, and combination treatment. The data in this study provide many theoretical bases to understand the molecular mechanisms of the cytotoxic effects of the Tan IIA combination with DDP in NSCLC cells. Tan IIA might be developed as a novel agent in postoperative adjuvant therapy combined with DDP and improved the sensibility of chemotherapeutics for NSCLC.

2 | MATERIALS AND METHODS

## 2.1 | Cell lines, culture conditions, and reagents

The NSCLC cell lines A549, PC9, H1299, and SPA-A1 were gifts from the State Key Laboratory of Oncology in South China. All cell lines were cultured in RPMI1640 (Gibco, Carlsbad, CA, USA) supplemented with 10% foetal bovine serum (Invitrogen Corp, Carlsbad, CA, USA), 100 U/ml penicillin and 100 U/ml streptomycin (Gino, Hangzhou, Zhejiang, China) in a humidified incubator at 37°C with 5% CO_2. Tan IIA and DDP were purchased from Sigma (St. Louis, MO, USA). Tan IIA was dissolved in dimethyl sulfoxide to make a 1-mM stock solution and stored at −20°C for future use. DDP was dissolved in physiological saline to make a 10-mM stock solution and stored at −20°C for future use; 740 Y-P was purchased from Beyotime Institute of Biotechnology and dissolved in physiological saline to make a 10-mM stock solution and stored at −20°C for future use.

2.2 | Cell viability assay

The antiproliferative effects of Tan IIA and DDP on NSCLC cell lines were detected using the CCK-8 kit (Dojindo Laboratories, 119 Kumamoto, Japan). A549, PC9, H1299, and SPA-A1 cells (8.0×10^3 cells each well) were seeded into 96-well plates. The cells were concurrently cultured with various concentrations of Tan IIA and DDP individually and concurrently. After treatment for 24, 48, or 72 hr, the cells were incubated for an additional 90 min with 10 μl of CCK-8 solution. Finally, the optical density was measured at 450 nm using a microculture plate reader (Thermo Scientific, Rockford, IL, USA). The proliferative inhibition rate was calculated using the following formula: proliferative inhibition rate = (1 − experimental group/control group) × 100%. The 50% inhibitory concentration (IC_{50}) value was calculated by non-linear regression analysis using SPSS 20.0 software.

2.3 | Synergy determination

The combination index (CI) was determined by isobologram analysis for the combination study, which was based on the Chou-Talalay method. The data obtained from the cell viability assay were standardized to the control group and presented as the % viability. Furthermore, the data were converted to the fraction affected (Fa; range 0–1; where Fa = 0 represents 100% viability and Fa = 1 represents 0% viability) and analysed using the CompuSyn™ programme (Biosoft, Ferguson, MO) based on the Chou-Talalay method. The CI
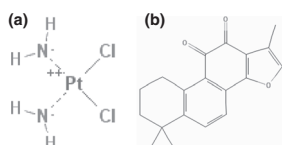
FIGURE 1 Two-dimensional structure of cisplatin (a) and Tanshione IIA (b) (obtained from PubChem compound http://pubchem.ncbi.nlm.nih.gov/)

values represent the modes of interaction between the two drugs. The CI < 1 indicates synergism, CI = 1 indicates an additive effect, and CI > 1 indicates antagonism.

2.4 | Wound healing assay

A549 and PC9 cells ($1 \times 10^6/1$ ml/well) in logarithmic phase were plated into six-well plates. After 24 hr, the adhesive cells were scratched along a straight line using a 200-μl pipette tip and then the scraped cells and cell debris were cleared three times with phosphate buffered saline (PBS). Fresh serum-free medium including various drugs was added to six-well plates, and the cells were allowed to repair the scratches for 24 hr. Images (magnification, ×10) were obtained at 0 and 24 hr at the same place that had been scratched. Then, Adobe Photoshop CS6 software was applied to measure the moving distance of cells.

2.5 | Transwell assay

The transwell filters (8-μm pore, 6.5-mm polycarbonate, Corning, NY, USA) were coated with a thin layer of Matrigel Basement Membrane Matrix (BD Biosciences, Bedford, MA). A549 and PC9 cells (3×10^4) in logarithmic phase were resuspended in 500-μl serum-free medium containing different drug treatments and plated on the upper compartment, and 800-μl complete medium including 10% FBS was added to the lower compartment. The transwell filters were placed in a humidified incubator at 37°C with 5% CO_2 for 24 hr. Next, the cells attached to the lower surface of the membrane were fixed with 4% paraformaldehyde at room temperature for 30 min and stained with 0.5% crystal violet. The cells on the upper surface of the filter were removed by wiping with a cotton swab. The number of stained cells on the lower surface was then counted using a microscope (magnification, ×100). Five fields were counted for each transwell filter.

2.6 | Cell cycle analysis

The Cell Cycle Detection Kit purchased from 4A Biotech Co., Ltd. was used to determine the cell cycle. A549 and PC9 cells ($5.0 \times 10^5/1$ ml/well) in logarithmic phase were plated into six-well plates with complete medium containing different drug treatments in a humidified incubator at 37°C with 5% CO_2 for 48 hr. The treated cells were collected and then washed with cold PBS. Subsequently, 70% cold ethanol was applied to immobilize the harvested cells at 4°C overnight. The cells were washed again with cold PBS and incubated with 100-μl RNase in a 37°C water bath for 30 min, followed by labelling with 400-μl propidium iodide and incubation for 30 min at room temperature in the dark. For each detection, at least 50,000 cells were evaluated. An ACEC NovoCyte flow cytometer equipped with Novoexpress (Becton Dickinson, San Jose, CA, USA) was used to detect the cell cycle.

2.7 | Apoptosis assay

The Annexin V-FITC apoptosis detection kit purchased from 4A Biotech Co., Ltd. was applied to detect cell apoptosis. A549 and PC9 cells ($5.0 \times 10^5/1$ ml/well) in logarithmic phase were plated in six-well plates and treated with different drugs for 48 hr. The treated cells were collected and washed with cold PBS after treatment. In accordance with the manufacturer's instructions, the cells were stained with Annexin V-FITC and propidium iodide for 30 min at room temperature in the dark, and the apoptosis rate of the treated cells was determined immediately after staining by using an ACEC NovoCyte flow cytometer equipped with Novoexpress (Becton Dickinson, San Jose, CA, USA).

2.8 | Mouse xenograft model

Equal numbers of A549 cells (2×10^6 cells) were resuspended in 100 ml of normal saline and subcutaneously injected into unilateral axillary fossae of 4-week-old nude mice (BALB/c-nu). The tumour volume was calculated with the formula $V = 0.5 \, ab^2$ (a, the longest tumour axis; b, the shortest tumour axis). When the volume of tumours reached 300 mm^3, the mice received an equal volume of Tan IIA (15 mg/kg), DDP (3 mg/kg), Tan IIA (7.5 mg/kg), and DDP (1.5 mg/kg) or vehicle (normal saline) via intraperitoneal injections twice a week. At the study end point, all mice were sacrificed, and tumours were excised. The animal studies were reviewed and approved by the SYSUCC Institutional Animal Care and Usage Committee. All experimental procedures involving animals were performed according to the Guidelines for the Care and Use of Laboratory Animals (NIH publications Nos. 80–23, revised 1996).

2.9 | Potential target recognition based on PharmMapper

PharmMapper (http://lilab.ecust.edu.cn/pharmmapper/index.php), is supported up by a large, in-house repertoire of a pharmacophore database extracted from all the targets in TargetBank, DrugBank, BindingDB, and PDTD. More than 7,000 receptor-based pharmacophore models (covering 1,627 drug targets information, 459 of which are human protein targets) are stored and accessed by PharmMapper. First, SDF of Tan IIA is downloaded from PubChem compound (https://www.ncbi.nlm.nih.gov/pccompound/) and then uploaded to PharmMapper. Following proper parameter setting, target identification is then carried out, and the Top 300 potential protein target information is obtained.

2.10 | KEGG pathway analysis

Based on KEGG Mapper (https://www.kegg.jp/kegg/tool/map_pathway2.html), the Search&Color Pathway is an advanced version of the KEGG pathway mapping tool, where given objects (genes, proteins, compounds, glycans, reactions, drugs, etc.) are searched against KEGG

pathway maps and discovered objects. First, *Homo sapiens* are selected, and then the Top 300 potential protein targets are uploaded; the information of the Top 100 potential pathway is obtained. A parameter enrichment gene count ≥2, and hypergeometric test significance threshold $p < .05$ are used.

2.11 | Molecular docking

To understand the potential interactions between the tested drugs and the selected proteins, a molecular docking algorithm was applied in this study with Discovery Studio (DS) 2.5. The two dimensional structures of Tan IIA and DDP were found in the PubChem database (http://pubchem.ncbi.nlm.nih.gov/), under the PubChem compound ID of 164676 and 441203, respectively. The 3D structure of phosphatidylinositol 3-kinase (PI3K; PDB-ID: 4urk), Akt (PDB-ID: 3o96), Caspase-3 (PDB-ID: 3kjf), and Bcl-2 (PDB-ID: 4lvt) targeted proteins could be acquired from the Protein Data Bank (PDB http://www.rcsb.org/pdb/home/home.do). The virtual docking procedures with DS 2.5 were as follows: First, the water molecules in the tested proteins were removed and refined with CHARMM on the targeted proteins and selected ligands. Second, the possible active sites of the tested proteins based on endogenous ligands were automatically determined with the algorithm. Third, the drugs, and selected ligands, were docked into the binding pocket of the tested proteins. The docking model of the drugs and the tested proteins was then examined by the module. Before performing the procedure, the root mean square deviation was calculated as verification for the selection of the two modules (CDOCKER and Libdock) in DS 2.5.

2.12 | Western blot analysis

A549 and PC9 cells in logarithmic phase were treated with different drugs for 48 hr. After treatment, the A549 and PC9 cells were harvested and lysed with lysis buffer. The cell lysates were incubated on ice for 30 min and then centrifuged at 12,000g for 10 min at 4°C. The supernatants were collected and protein content measured using BCA protein assay kit (Beyotime, Jiangsu, China). All selected protein extracts of the tested cells were separated by 10% sodium dodecyl sulfate-polyacrylamide gel electrophoresis and transferred to polyvinylidenedifluoride membranes (0.22 μm, Millipore, MA, USA). After blocking for 1 hr in 5% skim milk, the polyvinylidenedifluoride membranes were incubated overnight at 4°C with primary antibodies (p-PI3K 1:1,000, PI3K 1:1,000, p-Akt 1:1,000, Akt 1:1,000, Caspase-3 1:1,000, cleaved Caspase-3 1:1,000, Bcl-2 1:1,000, Bax 1:1,000, and glyceraldehyde 3-phosphate dehydrogenase 1:8,000). All primary antibodies were obtained from Cell Signaling Technology (Danvers, MA, USA). Following washing three times with Tris-buffered saline including 0.1% Tween-20 (TBST), the membranes were incubated with horseradish peroxidase-conjugated secondary antibodies (Cell Signaling Technology, Danvers, MA, USA) at room temperature for 1 hr. After washing again with TBST, the immunoreactivity of the membranes was detected using Bio-Rad-Image-Lab with an electrochemiluminescence system (Thermo Fisher Scientific, MA, USA). The densitometry of the protein bands were measured using the Image J (NIH image software) and normalized to their relevant controls.

2.13 | Statistical analysis

All experiments were repeated at least three times. Data are shown as the mean ± *SD* and were analysed using GraphPad Prism 6.02 software (San Diego, CA, USA), excluding the IC$_{50}$ values that were calculated using SPSS 20.0 software. Differences between groups were analysed using Student's *t* test. A *p* value of .05 or less was considered significant.

3 | RESULTS

3.1 | Cotreatment of Tan IIA and DDP synergistically inhibited the proliferation of NSCLC cells

Both Tan IIA and DDP were observed to inhibit NSCLC cell proliferation in a dose-dependent manner. Following 48 hr of treatment, the IC$_{50}$ values of Tan IIA for the A549, PC9, H1299, and SPA-A1 cell lines were 12.41, 11.43, 10.22, and 10.73 μM, respectively. Those of DDP were 0.41, 0.42, 0.31, and 0.36 μM, respectively (Figure 2).

In agreement with the IC$_{50}$ of Tan IIA and DDP, we set up the combination group at a fixed molar ratio of 20:1 (Tan IIA: DDP) for a 48-hr treatment. In comparison with the individual drug treatment, the drug combination treatment resulted in a stronger suppressive effect on cell proliferation. The synergism of the drug combination treatment was observed in A549, PC9, H1299, and SPA-A1 cell lines, regardless of the Fa value. The summary of CI and the concentration of the separate drugs used in combination at 50% Fa are depicted in Table 1.

3.2 | Cotreatment of Tan IIA and DDP synergistically inhibited the migration and invasion of NSCLC cells

To identify the combination of Tan IIA and DDP that achieved maximal biological function, we utilized the wound healing assay and transwell assay to study migration and invasion ability of A549 and PC9 cells. Figure 3 demonstrates that both the migration distances and invasive cell numbers were significantly decreased following 24 hr of drug treatment. In addition, the combination treatment exhibited the smallest migration distance and invasive cell number.

3.3 | Cotreatment of Tan IIA and DDP synergistically arrested the cell cycle of NSCLC cells

Following verification of the antiproliferative effect of Tan IIA and DDP, we utilized flow cytometry (FCM) to analyse the cell cycle phases of the treated NSCLC cells. As shown in Figure 4, Tan IIA
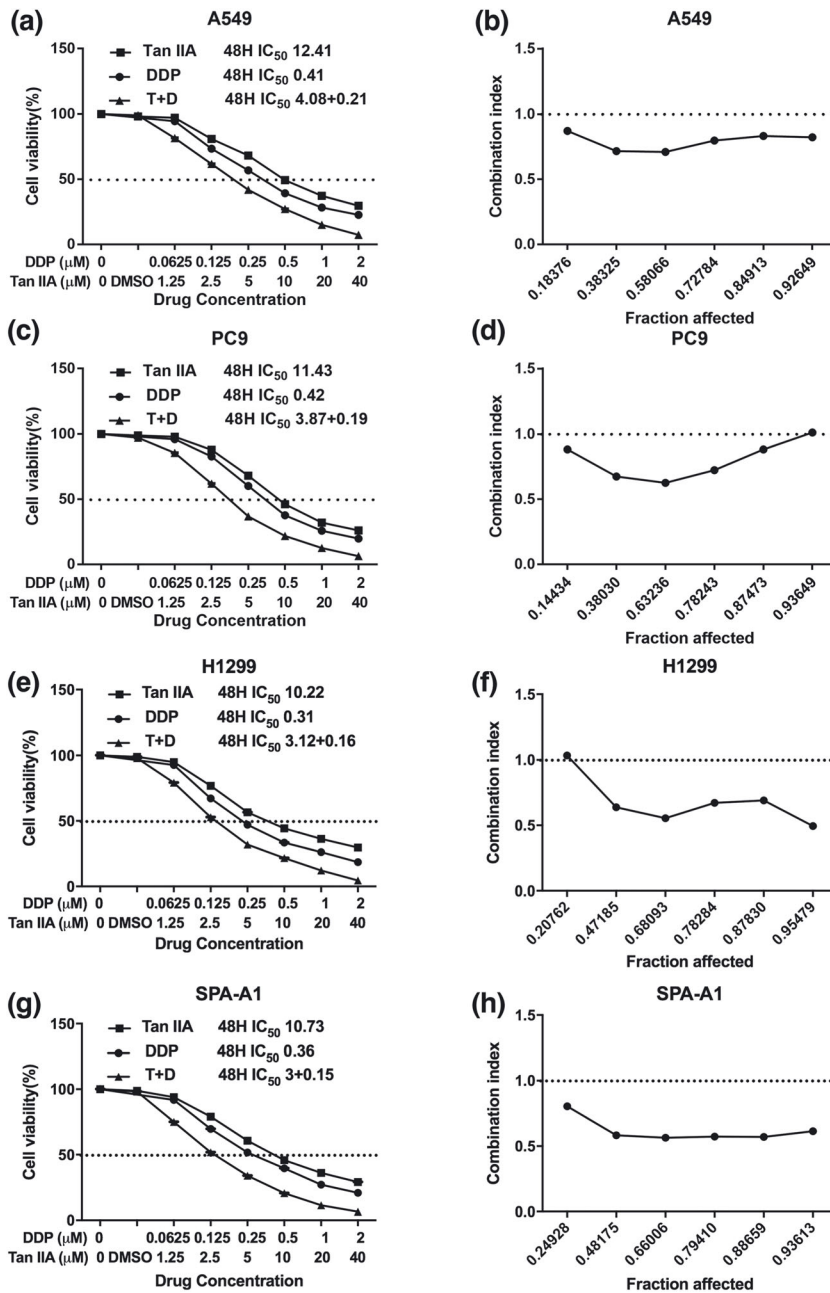
FIGURE 2 Proliferative inhibitory effect of Tan IIA, DDP, and the combination treatment on non-small-cell lung cancer cells. Drug concentration-cell viability curves were generated as the viable cell percentage based on the cell viability assay (a, c, e, g). Synergistic effects between Tan IIA and DDP are presented as Fa-CI plots (b, d, f, h). Data are from three repeated experiments with quadruplicate wells (mean ± SD). *p < .05, **p < .01, or ***p < .001 versus the control group. DDP, cisplatin; Tan IIA, Tanshione IIA

arrested A549 and PC9 cells at G1 phase, whereas DDP arrested A549 and PC9 cell at the S and G2 phase, and the combination of Tan IIA with DDP primarily arrested the cell cycle at S phase in A549cells and S and G2 phase in PC9 cells.

3.4 | Cotreatment of Tan IIA and DDP synergistically induced apoptosis of NSCLC cells

As depicted in Figure 5, both the single drug treatment and the drug combination increased the proportion of early and late apoptosis in A549 and PC9 cells. Furthermore, the combination of Tan IIA with DDP was found to more potently induce apoptosis in comparison

to the single treatment (Tan IIA + DDP vs. Tan IIA, ***0.0003; and Tan IIA + DDP vs. DDP, ***0.0005).

3.5 | Cotreatment of Tan IIA and DDP synergistically inhibited A549 cell xenograft tumour growth

We next studied the effect of Tan IIA and DDP on xenograft ESCC tumour growth. The experimental set-up, including A549 cell inoculation and drug treatment, is depicted in Figure 6. In the control group, xenograft tumours were observed to grow faster with a significantly greater tumour volume compared with the group that was treated with the tested drugs. In comparison to the Tan IIA and DDP monotherapy groups, the combined therapy using Tan IIA and

TABLE 1 Summary of CI value and the concentration of separate drugs in combination at 50% Fa

Drug combination	Fa = 0.5			
	A549	PC9	H1299	SPA-A1
DDP + Tan IIA				
CI	0.78348	0.75867	0.73588	0.64470
DDP (μM)	0.20769	0.20249	0.16046	0.14853
Tan IIA (μM)	4.15388	4.04975	3.20926	2.97054

Abbreviations: CI, combination index; DDP, cisplatin; Fa, fraction affected; Tan IIA, Tanshinone IIA.

DDP significantly inhibited tumour growth (Tan IIA + DDP vs. Tan IIA, **0.006; and Tan IIA + DDP vs. DDP, **0.007). Taken together, these data suggested that Tan IIA could also function to effectively increase the antitumour effect of DDP in vivo.

3.6 | Potential target proteins of Tan IIA and the KEGG pathway analysis

Using PharmaMapper, we obtained the Top 300 potential protein target information for Tan IIA (Table S1), and then the KEGG pathway analysis reminded us that Tan IIA might mainly influence the PI3K-Akt signalling pathway, as shown in Figure 7. We also utilized molecular docking to study the potential interactions between the tested drugs and PI3K/Akt signalling pathway. Molecular docking analysis demonstrated that both Tan IIA and DDP could be docked into the active site of PI3K, Akt, Caspase-3, and Bcl-2 in the binding pocket. Tan IIA and DDP were shown to form H-bonds or π-π interactions via different residues with PI3K, Akt, Caspase-3, and Bcl-2 in 10 random poses.

3.7 | Tan IIA combined with DDP synergistically decreased the activity of the PI3K/Akt signalling pathway in NSCLC cells

To explore the involved signal pathway, we performed western blotting to measure the levels of PI3K, p-PI3K, Akt, p-Akt, Caspase-3, cleaved Caspase-3, Bcl-2, and Bax in the single drug treatment and drug combination groups in A549 cells. As demonstrated in Figure 8, both single drug treatment and drug combination upregulated Bax and cleaved Caspase-3 expression levels but downregulated p-PI3K, p-Akt, Caspase-3, and Bcl-2 expression levels, with total Akt, PI3K, and glyceraldehyde 3-phosphate dehydrogenase levels remaining the same. Importantly, the effect in the drug combination groups revealed a significant difference compared with the single drug treatment groups (Tan IIA + DDP vs. Tan IIA, **$p < .01$; and Tan IIA + DDP vs. DDP, **$p < .01$). Next, we activated the PI3K/Akt signalling pathway through the PI3K activator (740 Y-P), and the inhibitory effect of combination therapy on the signalling pathway was partially recovered (**$p < .01$ in p-PI3K, p-Akt, Caspase-3, Bcl-2, Bax, and cleaved Caspase-3 for 740 Y-P + Tan IIA + DDP vs. Tan IIA + DDP group, but 0.065 in p-PI3K and 0.074 in p-Akt), as shown in Figure 8.
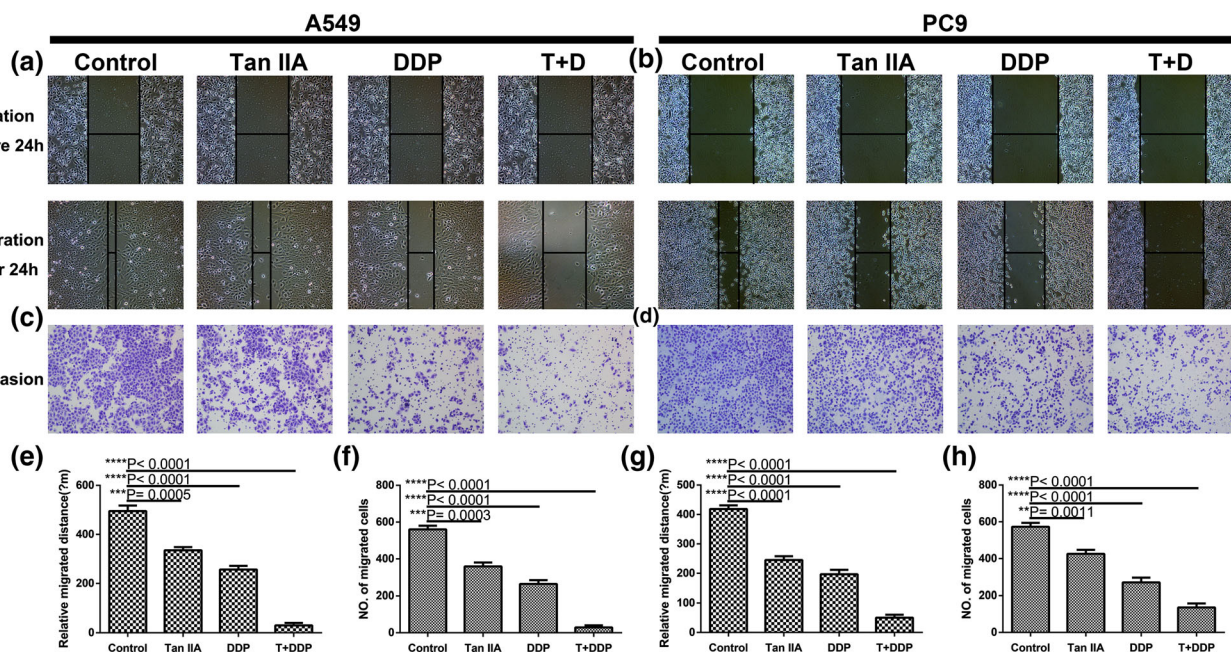
FIGURE 3 Tan IIA and DDP suppress the migration and invasion ability of A549 and PC9 cells. Representative images of wound healing (a, b) and transwell assays (c, d) following 24 hr of treatment with 10-μM Tan IIA, 0.5-μM DDP alone, and 0.2-μM DDP and 4-μM Tan IIA in combination. Histograms depict the average migrated distance (e, g) and the number of invasive cells (f, h), respectively. All data are shown as the mean ± SD of three independent experiments. **$p < .01$ or ***$p < .001$ versus the control group (magnification, ×100; scale bars, 100 μm). DDP, cisplatin; Tan IIA, Tanshione IIA [Colour figure can be viewed at wileyonlinelibrary.com]
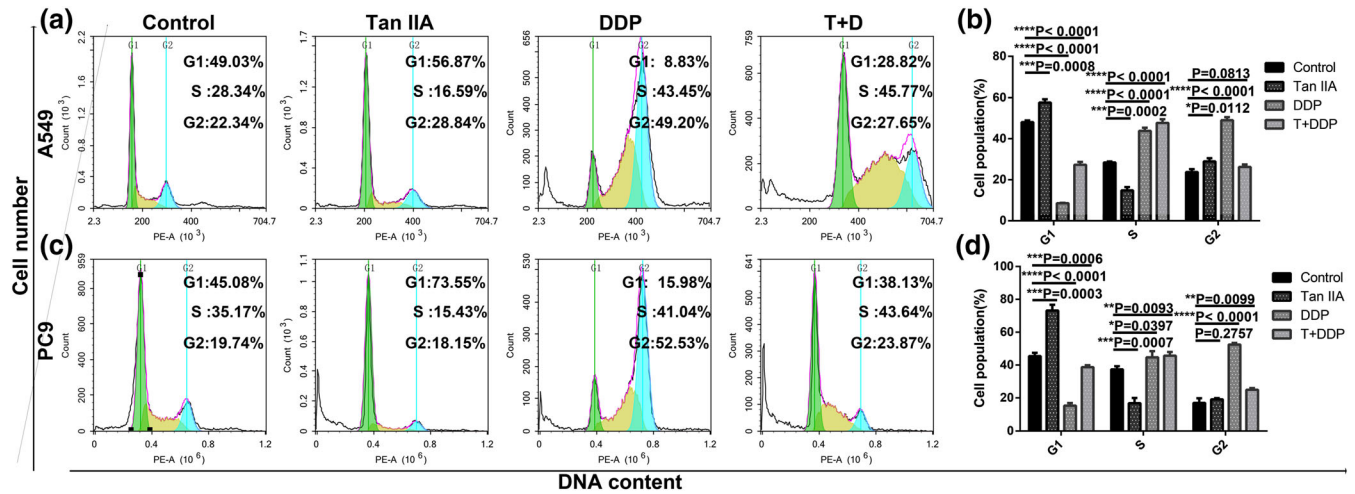
FIGURE 4 Effect of Tan IIA and DDP alone and in combination on cell cycle arrest. The percentage of cells in the G1, S, or G2/M phase in A549 (a) or PC9 cells (c) treated with 10-μM Tan IIA, 0.5-μM DDP alone, and 0.2-μM DDP and 4-μM Tan IIA in combination for 48 hr. Data represent the cell population in cell cycle arrest of A549 (b) and PC9 (d) cells. All data are shown as the mean ± SD of three independent experiments. *p < .05, **p < .01, or ***p < .001 versus the control group. DDP, cisplatin; Tan IIA, Tanshione IIA [Colour figure can be viewed at wileyonlinelibrary.com]
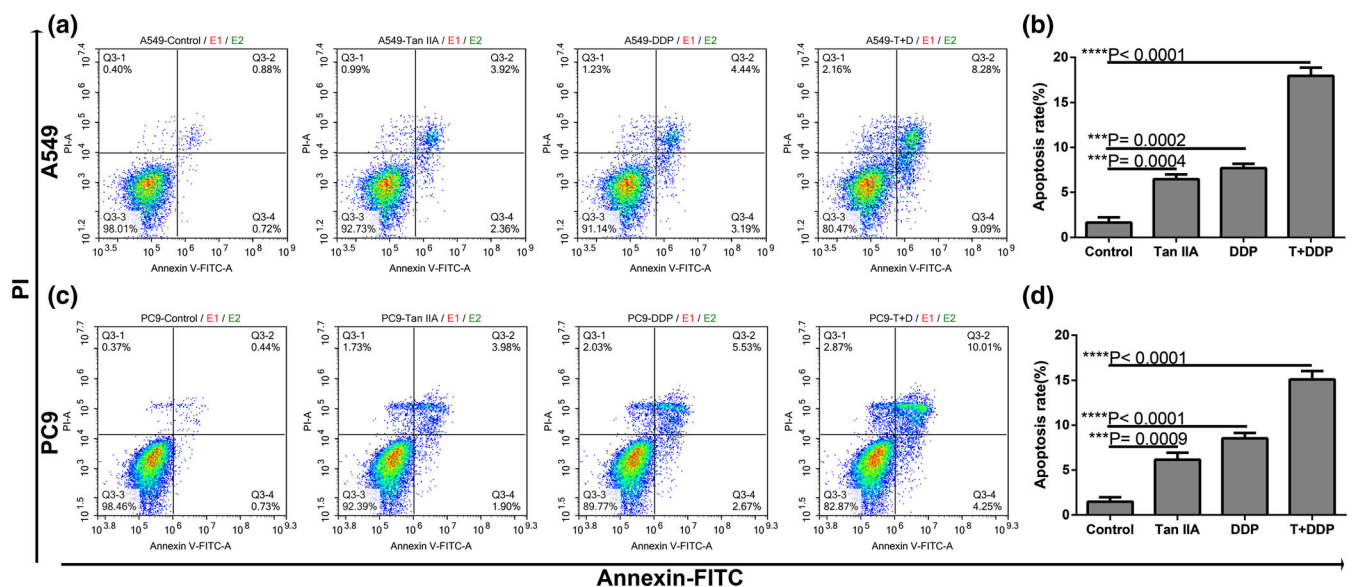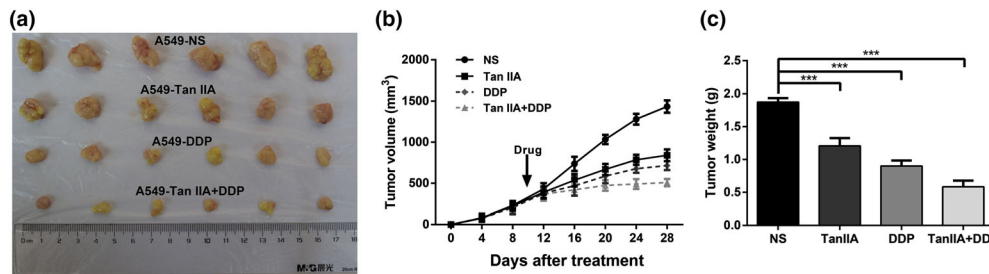

FIGURE 5 Effect of Tan IIA, DDP alone and in combination on apoptosis. Representative profiles showing apoptosis in A549 (a) or PC9 cells (c) treated with 10-μM Tan IIA, 0.5-μM DDP alone, and 0.2-μM DDP and 4 μM Tan IIA in combination for 48 hr. Data represent the cell population in cell cycle arrest of A549 (b) and PC9 (d) cells. All data are shown as the mean ± SD of three independent experiments. ***p < .001 versus the control group. DDP, cisplatin; Tan IIA, Tanshione IIA [Colour figure can be viewed at wileyonlinelibrary.com]

4 | DISCUSSION

In this study, we report the effect of the combination of Tan IIA with DDP on NSCLC, which may be developed further as a possible new therapeutic adjuvant treatment according to the current challenge of NSCLC treatment. Numerous researchers have focused on natural extracts owing to the success of artemisinin (qinghaosu) and arsenic (III) oxide (As_2O_3) in the clinic. Given their safety, long-term use, and ability to target multiple pathways, there is a renewed

interest in understanding the molecular mechanisms underlying their activity.

Our previous studies have also provided evidence of some natural agents with potential antitumour activity in combination with other therapeutic drug, such as Tan IIA (Xie et al., 2016) and matrine (Liao et al., 2017). However, there is no evidence at the cellular level or from animal models demonstrating such an effect of the combination of Tan IIA with DDP on NSCLC progression. The study presented herein indicates that the combination of Tan IIA with DDP diminishes

FIGURE 6 Ability of Tan IIA, DDP alone, and in combination to suppress the growth of A549 cells in vivo. Tumours derived from A549 cells in six male nude mice are presented (a). The tumour volume of all groups was measured every 4 days, beginning the first day after injection until the study end point. Data are shown as growth curves (b). The tumour mass of all groups was measured and compared, ***$p < .001$ versus the control group (c). DDP, cisplatin; Tan IIA, Tanshione IIA [Colour figure can be viewed at wileyonlinelibrary.com]

the growth and metastasis of NSCLC and suppresses the PI3K/Akt pathway, which may be a promising therapeutic strategy against NSCLC.

Based on the IC$_{50}$ values of the Cell Counting Kit-8 assay, we demonstrated that both Tan IIA and DDP had an inhibitory effect on the proliferation of A549, PC9, A322, and SPA-1 cells in a dose- and time-dependent manner. Compared with DDP, the inhibitory effect of Tan IIA was much weaker on the tested cell lines. As for the drug combination, it exerted synergistic inhibitory effects in A549, PC9, A322, and SPA-1 cells. Based on these results, we hypothesized that Tan IIA might potentiate the sensibility of NSCLC patients to DDP.

It has been reported that Tan IIA inhibits the migration and invasion ability of bladder cancer cells (Huang, Chang, Liao, & Chiu, 2017) and Tan IIA combined with adriamycin inhibits migration and invasion ability in NSCLC (Xie et al., 2016). Our findings also showed that Tan IIA combined with DDP could inhibit the migration and invasion ability of A549 and PC9 cells in a synergistic manner.

The current study also provides insight into the mechanism of the synergistic effect of Tan IIA in combination with DDP on the cell cycle distribution through the use FCM experiments in A549 and PC9 cells. FCM showed that both drug combination treatment and single DDP treatment caused S and G2 phase arrest in A549 and PC9 cells, whereas single Tan IIA treatment caused G1 phase arrest. Ma found that in the NSCLC cell line H1299, the proportion of cells in G1 phase was increased compared with the control following treatment with Tan IIA (4 μM, 48 hr; Ma et al., 2015). However, the effect of Tan IIA on the cell cycle distribution is still controversial. Different results were found using the renal cancer cell line 786-O, for which the percentage of cells in S phase was increased in a dose-dependent manner response to Tan IIA treatment (0, 6.79, 13.59, or 27.18 μM, 24 hr; Wei, Zhou, Hu, & Huang, 2012). These findings showed that low dosage Tan IIA might contribute to the cell cycle arrest at G1 phase, whereas high dosage Tan IIA might lead to S phase cell cycle blockage, which remains to be further explored.

Many studies have demonstrated that Tan IIA results in an increased apoptosis rate in NSCLC (Chiu & Su, 2010), and colorectal carcinoma (He & Gu, 2018). Furthermore, Zhao found that Tan IIA could potentiate the apoptosis rate of DDP in pharyngeal squamous cell carcinoma (Zhao et al., 2017). Our results also demonstrated that both Tan IIA and DDP were able to produce the same results in
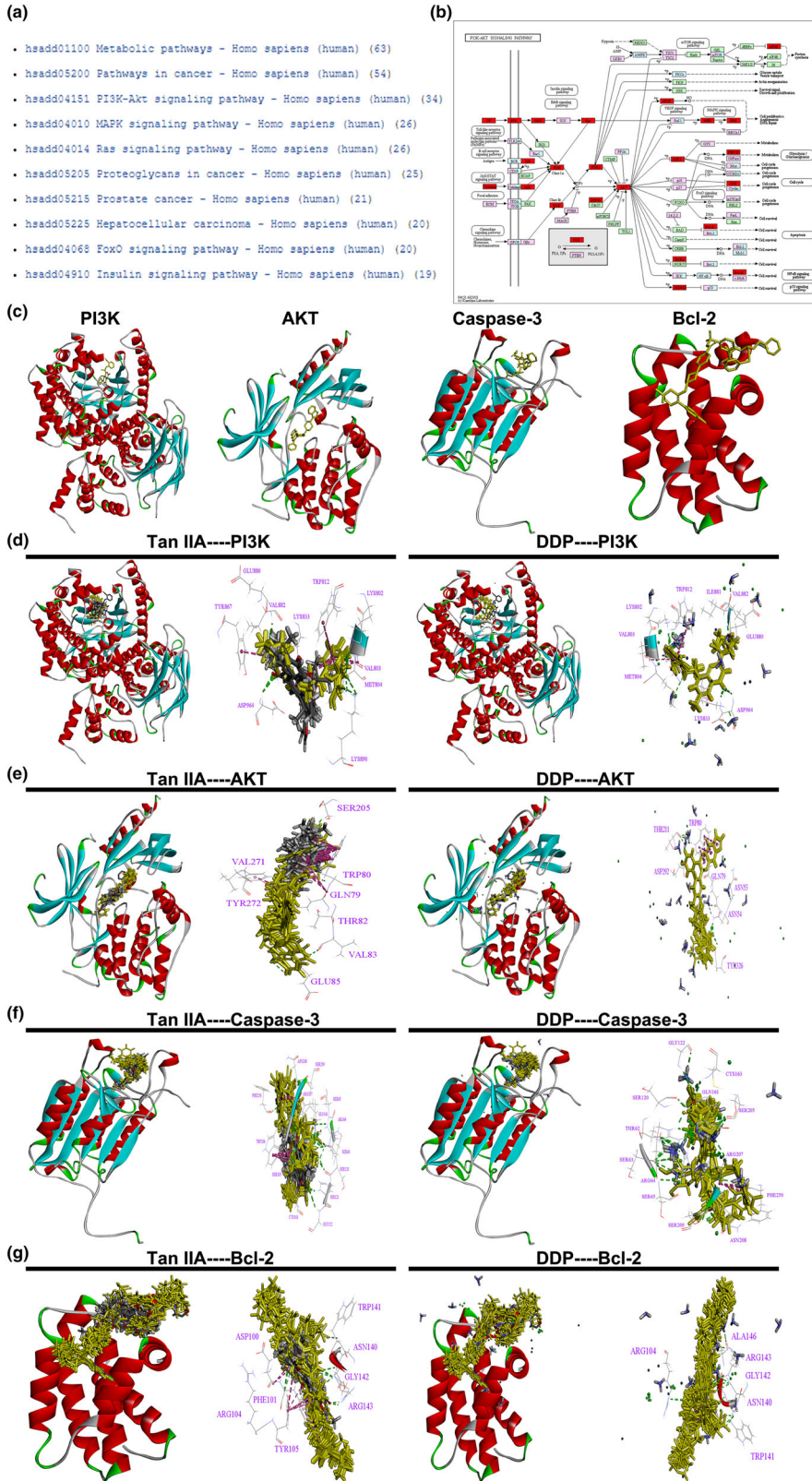
A549 and PC9 cells, and compared with single drug treatment, combined application of these two drugs can significantly increase the apoptosis rates. Taken together, these results suggest that the combination treatment of both Tan IIA and DDP could function to synergistically promote apoptosis.

Huang and his team found that Tan IIA induces intrinsic apoptosis in osteosarcoma cells both in vivo and in vitro (Huang, Huang, et al., 2017). Our results also showed that both Tan IIA and DDP could inhibit NSCLC xenograft tumour growth, and the combination of these two exerted more significant effects in vivo. Therefore, our results indicated that Tan IIA could function to effectively increase the antitumour effect of DDP in vivo.

Next, using PharmMapper (Wang et al., 2017), we obtained the Top 300 potential protein target information for Tan IIA, and the KEGG pathway analysis reminded us that Tan IIA might mainly influence the PI3K/Akt signalling pathway, which is consistent with some recent studies (Cao, Wang, Li, Zhang, & Qiao, 2018; Chen, 2015; Ding et al., 2017). Additionally, Su also reported that Tan IIA blocked the PI3K/Akt pathway in gastric carcinoma AGS cells both in vitro and in vivo (Su, 2018). Similarly, many recent studies also reported that inactivation of the PI3K/Akt pathway could enhance the chemosensitivity of NSCLC cells to DDP (Chen et al., 2017; Gong, Cui, Wang, Wang, & Han, 2018; Liu, Xing, & Rong, 2018; Shi, Pu, Zhou, Ning, & Bai, 2017; Xia, Li, Li, Lu, & Wu, 2018; Zhao et al., 2018). Therefore, we conjectured that Tan IIA might block the PI3K/Akt pathway and then enhance the anticancer ability of DDP in NSCLC.

PI3K activity is stimulated by diverse oncogenes and growth factor receptors, and elevated PI3K signalling is considered a hallmark of cancer (Fruman et al., 2017). Additionally, Akt is an important downstream effector of oncogenic PI3K signalling and regulates several pathways, including inhibition of apoptosis, stimulation of cell growth, and modulation of cellular metabolism (Fruman et al., 2017). Furthermore, it is well established that the PI3K/Akt pathway is one of the most important oncogenic pathways in almost all kinds of human cancers, being vital to the growth and survival of cancer cells, as well as disease initiation and development, including tumorigenesis, proliferation, invasion, cell cycle progression, inhibition of apoptosis, angiogenesis, metastasis, and chemoresistance in cancer cells (Zhang, Yu, Yan, Wang, & Wang, 2015).

(a)

- hsadd01100 Metabolic pathways - Homo sapiens (human) (63)
- hsadd05200 Pathways in cancer - Homo sapiens (human) (54)
- hsadd04151 PI3K-Akt signaling pathway - Homo sapiens (human) (34)
- hsadd04010 MAPK signaling pathway - Homo sapiens (human) (26)
- hsadd04014 Ras signaling pathway - Homo sapiens (human) (26)
- hsadd05205 Proteoglycans in cancer - Homo sapiens (human) (25)
- hsadd05215 Prostate cancer - Homo sapiens (human) (21)
- hsadd05225 Hepatocellular carcinoma - Homo sapiens (human) (20)
- hsadd04068 FoxO signaling pathway - Homo sapiens (human) (20)
- hsadd04910 Insulin signaling pathway - Homo sapiens (human) (19)

(b)

(c)

PI3K AKT Caspase-3 Bcl-2

(d)

Tan IIA----PI3K DDP----PI3K

(e)

Tan IIA----AKT DDP----AKT

(f)

Tan IIA----Caspase-3 DDP----Caspase-3

(g)


Tan IIA----Bcl-2 DDP----Bcl-2

FIGURE 7 KEGG pathway analysis of Tan IIA and the PI3K/AKT signalling pathway. The Top 10 signalling pathways of Tan IIA in KEGG pathway analysis (a). The PI3K/AKT signalling pathway and the potential target protein (red) of Tan IIA (b). The 3D crystal structure of human PI3K, AKT, Caspase-3, and Bcl-2 with an endogenous ligand (PDB-ID: 4urk, 3o96, 3kjf, 4lvt) (c). Ten random poses of Tan IIA and DDP docked in the active site of 4urk (d). Ten random poses of Tan IIA and DDP docked in the active site of 3o96 (e). Ten random poses of Tan IIA and DDP docked in the active site of 3kjf (f). Ten random poses of Tan IIA and DDP docked in the active site of 4lvt (g). DDP, cisplatin; Tan IIA, Tanshione IIA; P13K, phosphatidylinositol 3-kinase [Colour figure can be viewed at wileyonlinelibrary.com]

Our western blot results revealed that the drug treatment gave rise to distinctly high expressions levels of cleaved-Caspase-3 and Bax but low expressions levels of Bcl-2, Caspase-3, p-Akt, and p-PI3K proteins, with total Akt and PI3K protein expression remaining nearly the same. The effects of the drug combination treatment showed a more significant difference compared with the single drug treatment. Thus, we hypothesized that the drug induced pro-apoptotic process was likely associated with the down-regulation of the PI3K/Akt signalling pathway. Bax and cleaved Caspase-3 were up-regulated, suggesting that the mitochondrial apoptotic pathway was also involved in Tan
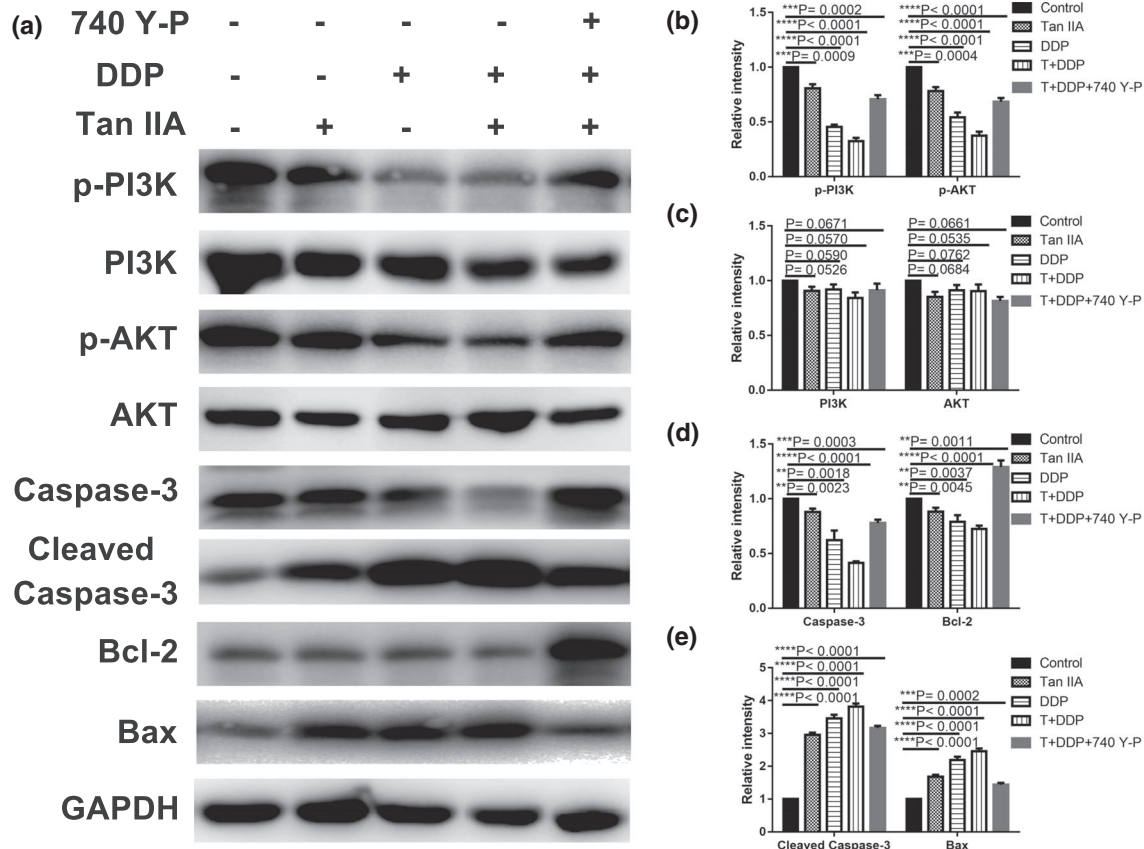
FIGURE 8 Suppressive effect of Tan IIA, DDP, and the combination on the PI3K/AKT signalling pathway in A549 cells. Protein expression levels of p-PI3K, PI3K, p-Akt, Akt, Caspase-3, cleaved Caspase-3, Bcl-2, Bax, and GAPDH in A549 cells treated with 10-μM Tan IIA, 0.5-μM DDP alone, 0.2-μM DDP, and 4-μM Tan IIA in combination with or without 30 μM 740 Y-P for 48 hr (a). Histograms depicting the relative grey value of the related proteins measured using Image J (b–e). All data are shown as the mean ± SD of three independent experiments. **$p < .01$ or ***$p < .001$ versus the control group. DDP, cisplatin; GAPDH, glyceraldehyde 3-phosphate dehydrogenase; Tan IIA, Tanshione IIA; P13K, phosphatidylinositol 3-kinase

IIA-induced A549 cell death, which is consistent with many other studies.

These investigations indicated that inhibition of the PI3K/Akt signalling cascade could serve as an effective strategy for the treatment of NSCLC. Agents (such as Tan IIA) targeting the apoptosis pathway might play crucial roles as potential drug targets in cancer management, minimizing adverse effects, maximizing clinical outcomes, and helping to improve patients' quality of life.

To provide further evidence to allow an in-depth understanding of the probable mechanisms of the combination of Tan IIA and DDP, further studies should be conducted. For example, the probable molecular mechanisms involving the PI3K/Akt signalling pathway must be assessed using antagonist antibodies. Based on the results of this study, we believe Tan IIA should be further developed as a possible new therapeutic adjuvant treatment for NSCLC. Our findings demonstrated that the combination treatment of Tan IIA with DDP could function to synergistically inhibit NSCLC cells through down-regulation of the PI3K/Akt signalling pathway. In the combination treatment regimen, Tan IIA was able to improve the sensitivity of NSCLC cells to DDP and reduce the DDP dosage, thereby potentially reducing its side effects. This finding indicated that Tan IIA could serve as a novel option in combinative therapy for NSCLC treatment.

CONFLICT OF INTEREST

The authors declare that they have no competing interests.

AVAILABILITY OF DATA AND MATERIALS

All data generated or analysed during this study are included in this published article.

CONSENT FOR PUBLICATION

Consent to publish has been obtained from all authors.

ETHICS APPROVAL AND CONSENT TO PARTICIPATE

All aspects of this study were approved by the medical ethics committee of Sun Yat-sen University Cancer Center. All animal studies were performed with approval from the Institutional Animal Care and Use Committee of Sun Yat-sen University.

ORCID

Li-Zhu Lin https://orcid.org/0000-0001-8283-6554

REFERENCES

Cao, Y. F., Wang, S. F., Li, X., Zhang, Y. L., & Qiao, Y. J. (2018). The anticancer mechanism investigation of Tanshinone IIA by pharmacological clustering in protein network. *BMC Systems Biology*, *12*(1), 90. https://doi.org/10.1186/s12918-018-0606-6

Chen, L. M., Song, T. J., Xiao, J. H., Huang, Z. H., Li, Y., & Lin, T. Y. (2017). Tripchlorolide induces autophagy in lung cancer cells by inhibiting the PI3K/AKT/mTOR pathway and improves cisplatin sensitivity in A549/DDP cells. *Oncotarget*, *8*(38), 63911–63922.

Chen, S. J. (2015). Drug-target networks for Tanshinone IIA identified by data mining. *Chinese Journal of Natural Medicines*, *13*(10), 751–759. https://doi.org/10.1016/S1875-5364(15)30075-3

Chen, Z., & Xu, H. (2014). Anti-inflammatory and immunomodulatory mechanism of Tanshinone IIA for atherosclerosis. *Evidence-based Complementary and Alternative Medicine: Ecam*, *2014*(267976), 1–6. https://doi.org/10.1155/2014/267976

Chiu, T. L., & Su, C. C. (2010). Tanshinone IIA induces apoptosis in human lung cancer A549 cells through the induction of reactive oxygen species and decreasing the mitochondrial membrane potential. *International Journal of Molecular Medicine*, *25*(2), 231–236.

Chiu, T. L., & Su, C. C. (2017). Tanshinone IIA increases protein expression levels of PERK, ATF6, IRE1alpha, CHOP, caspase3 and caspase12 in pancreatic cancer BxPC3 cell-derived xenograft tumors. *Molecular Medicine Reports*, *15*(5), 3259–3263. https://doi.org/10.3892/mmr.2017.6359

Ding, L., Ding, L., Wang, S., Wang, S., Wang, W., Wang, W., … Qi, L. (2017). Tanshinone IIA affects autophagy and apoptosis of glioma cells by inhibiting phosphatidylinositol 3-kinase/Akt/mammalian target of rapamycin signaling pathway. *Pharmacology*, *99*(3–4), 188–195. https://doi.org/10.1159/000452340

Fruman, D. A., Chiu, H., Hopkins, B. D., Bagrodia, S., Cantley, L. C., & Abraham, R. T. (2017). The PI3K pathway in human disease. *Cell*, *170*(4), 605–635. https://doi.org/10.1016/j.cell.2017.07.029

Galluzzi, L., Vitale, I., Michels, J., Brenner, C., Szabadkai, G., Harel-Bellan, A., … Kroemer, G. (2014). Systems biology of cisplatin resistance: Past, present and future. *Cell Death & Disease*, *5*, e1257. https://doi.org/10.1038/cddis.2013.428

Gong, T., Cui, L., Wang, H., Wang, H., & Han, N. (2018). Knockdown of KLF5 suppresses hypoxia-induced resistance to cisplatin in NSCLC cells by regulating HIF-1alpha-dependent glycolysis through inactivation of the PI3K/Akt/mTOR pathway. *Journal of Translational Medicine*, *16*(1), 164. https://doi.org/10.1186/s12967-018-1543-2

Guo, Z., Yan, M., Chen, L., Fang, P., Li, Z., Wan, Z., … Zhang, B. (2018). Nrf2-dependent antioxidant response mediated the protective effect of Tanshinone IIA on doxorubicin-induced cardiotoxicity. *Experimental and Therapeutic Medicine*, *16*(4), 3333–3344.

He, L., & Gu, K. (2018). Tanshinone IIA regulates colorectal cancer apoptosis via attenuation of Parkin-mediated mitophagy by suppressing AMPK/Skp2 pathways. *Molecular Medicine Reports*, *18*(2), 1692–1703.

Huang, S. T., Huang, C. C., Huang, W. L., Lin, T. K., Liao, P. L., Wang, P. W., … Chuang, J. H. (2017). Tanshinone IIA induces intrinsic apoptosis in osteosarcoma cells both in vivo and in vitro associated with mitochondrial dysfunction. *Scientific Reports*, *7*, 40382. https://doi.org/10.1038/srep40382

Huang, S. Y., Chang, S. F., Liao, K. F., & Chiu, S. C. (2017). Tanshinone IIA inhibits epithelial-mesenchymal transition in bladder cancer cells via modulation of STAT3-CCL2 signaling. *International Journal of Molecular Sciences*, *18*(8). https://doi.org/10.3390/ijms18081616

Jin, Z., Guan, L., Song, Y., Xiang, G. M., Chen, S. X., & Gao, B. (2016). MicroRNA-138 regulates chemoresistance in human non-small cell lung cancer via epithelial mesenchymal transition. *European Review for Medical and Pharmacological Sciences*, *20*(6), 1080–1086.

Li, K., & Lai, H. (2017). TanshinoneIIA enhances the chemosensitivity of breast cancer cells to doxorubicin through down-regulating the expression of MDR-related ABC transporters. *Biomedicine & pharmacotherapy = Biomedecine & pharmacotherapie*, *96*, 371–377. https://doi.org/10.1016/j.biopha.2017.10.016

Liao, X. Z., Tao, L. T., Liu, J. H., Gu, Y. Y., Xie, J., Chen, Y., … Mo, S. L. (2017). Matrine combined with cisplatin synergistically inhibited urothelial bladder cancer cells via down-regulating VEGF/PI3K/Akt signaling pathway. *Cancer Cell International*, *17*, 124. https://doi.org/10.1186/s12935-017-0495-6

Liu, J., Xing, Y., & Rong, L. (2018). miR-181 regulates cisplatin-resistant non-small cell lung cancer via downregulation of autophagy through the PTEN/PI3K/AKT pathway. *Oncology Reports*, *39*(4), 1631–1639.

Lv, C., Zeng, H. W., Wang, J. X., Yuan, X., Zhang, C., Fang, T., … Zhang, W. D. (2018). The antitumor natural product Tanshinone IIA inhibits protein kinase C and acts synergistically with 17-AAG. *Cell Death & Disease*, *9*(2), 165. https://doi.org/10.1038/s41419-017-0247-5

Ma, Z. L., Zhang, B. J., Wang, D. T., Li, X., Wei, J. L., Zhao, B. T., … Jin, Y. X. (2015). Tanshinones suppress AURKA through up-regulation of miR-32 expression in non-small cell lung cancer. *Oncotarget*, *6*(24), 20111–20120. https://doi.org/10.18632/oncotarget.3933

Shi, H., Pu, J., Zhou, X. L., Ning, Y. Y., & Bai, C. (2017). Silencing long noncoding RNA ROR improves sensitivity of non-small-cell lung cancer to cisplatin resistance by inhibiting PI3K/Akt/mTOR signaling pathway. *Tumour Biology: The Journal of the International Society for Oncodevelopmental Biology and Medicine*, *39*(5). 1010428317697568

Siegel, R. L., Miller, K. D., & Jemal, A. (2017). Cancer statistics, 2017. *CA: a Cancer Journal for Clinicians*, *67*(1), 7–30. https://doi.org/10.3322/caac.21387

Su, C. C. (2018). Tanshinone IIA inhibits gastric carcinoma AGS cells by decreasing the protein expression of VEGFR and blocking Ras/Raf/MEK/ERK pathway. *International Journal of Molecular Medicine*, *41*(4), 2389–2396.

Sui, H., Zhao, J., Zhou, L., Wen, H., Deng, W., Li, C., … Li, Q. (2017). Tanshinone IIA inhibits beta-catenin/VEGF-mediated angiogenesis by targeting TGF-beta1 in normoxic and HIF-1alpha in hypoxic microenvironments in human colorectal cancer. *Cancer Letters*, *403*, 86–97. https://doi.org/10.1016/j.canlet.2017.05.013

Tsai, M. Y., Yang, R. C., Wu, H. T., Pang, J. H., & Huang, S. T. (2011). Anti-angiogenic effect of Tanshinone IIA involves inhibition of matrix invasion and modification of MMP-2/TIMP-2 secretion in vascular

endothelial cells. *Cancer Letters*, *310*(2), 198–206. https://doi.org/10.1016/j.canlet.2011.06.031

Wang, X., Shen, Y., Wang, S., Li, S., Zhang, W., Liu, X., … Li, H. (2017). PharmMapper 2017 update: A web server for potential drug target identification with a comprehensive target pharmacophore database. *Nucleic Acids Research*, *45*(W1), W356–W360. https://doi.org/10.1093/nar/gkx374

Webb, J. D., & Simon, M. C. (2010). Novel insights into the molecular origins and treatment of lung cancer. *Cell Cycle (Georgetown, Texas)*, *9*(20), 4098–4105. https://doi.org/10.4161/cc.9.20.13588

Wei, X., Zhou, L., Hu, L., & Huang, Y. (2012). Tanshinone IIA arrests cell cycle and induces apoptosis in 786-O human renal cell carcinoma cells. *Oncology Letters*, *3*(5), 1144–1148. https://doi.org/10.3892/ol.2012.626

Wohlkoenig, C., Leithner, K., Deutsch, A., Hrzenjak, A., Olschewski, A., & Olschewski, H. (2011). Hypoxia-induced cisplatin resistance is reversible and growth rate independent in lung cancer cells. *Cancer Letters*, *308*(2), 134–143. https://doi.org/10.1016/j.canlet.2011.03.014

Xia, A., Li, H., Li, R., Lu, L., & Wu, X. (2018). Co-treatment with BEZ235 enhances chemosensivity of A549/DDP cells to cisplatin via inhibition of PI3/Akt/mTOR signaling and downregulation of ERCC1 expression. *Oncology Reports*, *40*(4), 2353–2362.

Xie, J., Liu, J. H., Liu, H., Liao, X. Z., Chen, Y., Lin, M. G., … Mo, S. L. (2016). Tanshinone IIA combined with adriamycin inhibited malignant biological behaviors of NSCLC A549 cell line in a synergistic way. *BMC Cancer*, *16*(1), 899. https://doi.org/10.1186/s12885-016-2921-x

Zhang, J., Yu, X. H., Yan, Y. G., Wang, C., & Wang, W. J. (2015). PI3K/Akt signaling in osteosarcoma. *Clinica Chimica Acta; International Journal of Clinical Chemistry*, *444*, 182–192. https://doi.org/10.1016/j.cca.2014.12.041

Zhang, Y., Guo, S., Fang, J., Peng, B., Zhang, Y., & Cao, T. (2018). Tanshinone IIA inhibits cell proliferation and tumor growth by downregulating STAT3 in human gastric cancer. *Experimental and Therapeutic Medicine*, *16*(4), 2931–2937.

Zhao, M., Xu, P., Liu, Z., Zhen, Y., Chen, Y., Liu, Y., … Fang, W. (2018). Dual roles of miR-374a by modulated c-Jun respectively targets CCND1-inducing PI3K/AKT signal and PTEN-suppressing Wnt/beta-catenin signaling in non-small-cell lung cancer. *Cell Death & Disease*, *9*(2), 78. https://doi.org/10.1038/s41419-017-0103-7

Zhao, Y. X., Luo, D., Zhang, Y. H., Shen, B., Wang, B. X., & Sun, Z. F. (2017). The effect of Tanshinone A potentiates the effects of cisplatin in Fadu cells in vitro through downregulation of survivin. *Lin Chuang Er Bi Yan Hou Tou Jing Wai Ke Za Zhi = Journal of Clinical Otorhinolaryngology, Head, and Neck Surgery*, *31*(10), 781–784.

SUPPORTING INFORMATION

Additional supporting information may be found online in the Supporting Information section at the end of the article.